

**MIXED MATRIX MEMBRANES  
INCORPORATED WITH PALLADIUM  
NANOPARTICLES FOR HYDROGEN  
SEPARATION**

**HANI SHAZWANI BINTI MOHD SUHAIMI**

**UNIVERSITI SAINS MALAYSIA**

**2018**

**MIXED MATRIX MEMBRANES INCORPORATED WITH PALLADIUM  
NANOPARTICLES FOR HYDROGEN SEPARATION**

**by**

**HANI SHAZWANI BINTI MOHD SUHAIMI**

**Thesis submitted in fulfilment of the  
requirements for the degree of  
Doctor of Philosophy**

**AUGUST 2018**

## ACKNOWLEDGEMENT

In the name of Allah S.W.T., the most gracious and the most merciful.

I would like to express my most thankful to ALLAH S.W.T for the blessing of time, fortune and life for me to do my research work. All praise belongs to ALLAH S.W.T.

This thesis is the symbolism of continuous encouragements and love that I acquired from my affectionate parents, Mohd Suhaimi Bin Abu Bakar and Azimah Binti Omar, my caring in-laws, Bahari Bin Rantau and Norsirah Binti Abdol, my supportive and lovely husband, Mohd Ashriq Muzzammil, my dear children (Hasya Sofea and Afry Zharif) and all my family members. Special gratitude for their endless support and prays.

I would like to convey my highly appreciation to my supportive supervisor Associate Prof. Ir. Dr. Leo Choe Peng, for her nonstop assistance, expert guidance and invaluable knowledge, advices and ideas throughout this study. I would also like to extend my sincere thanks to my co-supervisor, Prof. Dr. Abdul Latif Bin Ahmad for his beneficial input and support. I am truly grateful to have the opportunity to work under their supervision.

I would also like to express my appreciation to the Dean and Deputy Deans of School of Chemical Engineering, USM for their constant support and help. My sincere thanks goes to all the respective lecturers, supportive technicians and

compassionate staffs in the School of Chemical Engineering, USM for their kind cooperation and sincere support throughout this project.

I aspire to express the deepest gratitude to all my beloved friends especially my postgraduate colleagues under supervision of Associate Prof. Ir. Dr. Leo Choe Peng (Nor Aini, Dr Usman, Siti Nadiah, David Yeo, Nor Naimah Rosyadah, Melvin Ng, Nur Haziyana and Nurul Izyatulikma) for their valuable time, supportive energy, unparalleled help and all beautiful moments together in this past years. Thank you very much and I hope that our friendship will last forever.

For the financial support, I wish to state my highest acknowledgement to USM for giving me supportive support via USM Fellowship scholarship. Special gratitude to Ministry of Higher Education Malaysia for granting financial support by providing MyPHd and FRGS (203.PJKIMIA.6071274). Finally, fundings provided by MOSTI and USM through Membrane Science and Technology Cluster (1001/PSF/8610013), Research University Individual Grant (1001/PJKMIA/811194) and Science Fund (06-01-05-SF0579) for conducting this work are gratefully recognized.

Alhamdulillah.

## TABLES OF CONTENTS

|                                       | <b>Page</b> |
|---------------------------------------|-------------|
| <b>ACKNOWLEDGEMENT</b>                | ii          |
| <b>TABLE OF CONTENTS</b>              | iv          |
| <b>LIST OF TABLES</b>                 | xi          |
| <b>LIST OF FIGURES</b>                | xiv         |
| <b>LIST OF ABBREVIATIONS</b>          | xxi         |
| <b>LIST OF SYMBOLS</b>                | xxv         |
| <b>ABSTRAK</b>                        | xxvii       |
| <b>ABSTRACT</b>                       | xxix        |
| <br>                                  |             |
| <b>CHAPTER ONE: INTRODUCTION</b>      |             |
| 1.1 Hydrogen demand and production    | 1           |
| 1.2 Hydrogen separation               | 10          |
| 1.3 Problem statement                 | 17          |
| 1.4 Objectives                        | 19          |
| 1.5 Scope of study                    | 20          |
| 1.6 Organization of the thesis        | 22          |
| <br>                                  |             |
| <b>CHAPTER TWO: LITERATURE REVIEW</b> |             |
| 2.1 Hydrogen-selective membrane       | 25          |
| 2.1.1 Polymeric membranes             | 30          |
| 2.1.1(a) Polysulfone                  | 31          |
| 2.1.1(b) Polybenzimidazole            | 34          |

|   |    |
|---|----|
| 2.1.2 Inorganic membranes   | 37 |
| 2.1.2(a) Dense metallic membrane  | 38 |
| 2.1.2(b) Microporous membranes  | 44 |
| 2.1.3 Mixed Matrix membranes  | 47 |
| 2.1.3(a) Effect of stabilizer on MMMs properties and<br>performance     | 56 |
| 2.1.3(b) Effect of filler loading on MMMs properties and<br>performance | 58 |
| 2.1.3(c) Effect of operating temperture on MMMs<br>performance          | 59 |
| 2.2 The application of membrane in biohydrogen system                   | 61 |
| 2.3 The uses and synthesis of Pd nanoparticles                          | 63 |
| 2.3.1 The role of Pd nanoparticles in H <sub>2</sub> economy            | 65 |
| 2.3.2 The synthesis of Pd nanoparticles                                 | 66 |
| <br><b>CHAPTER THREE: METHODOLOGY</b>                                   |    |
| 3.1 Introduction  | 71 |
| 3.2 Research flow   | 71 |
| 3.3 Materials and Chemicals   | 72 |
| 3.4 Synthesis of Pd nanoparticles precursor                             | 75 |
| 3.4.1 Synthesis of Pd/PEG   | 75 |
| 3.4.2 Synthesis of Pd/PVP   | 76 |
| 3.5 Characterization of Pd nanoparticles                                | 76 |
| 3.5.1 Transmission electron micrograph (TEM) analysis                   | 77 |
| 3.5.2 X-ray diffraction (XRD) analysis                                  | 77 |

|        |  |    |
|--------|--|----|
| 3.5.3  | Temperature programmed reduction (TPR) analysis              | 77 |
| 3.6    | Preparation of membrane                                      | 78 |
| 3.6.1  | PSf membrane solution preparation                            | 78 |
| 3.6.2  | PSf(Pd) MMMs solution preparation                            | 79 |
| 3.6.3  | Flat Sheet Membrane Casting for PSf membrane and PSf<br>MMMs | 79 |
| 3.6.4  | PBI membrane solution preparation                            | 80 |
| 3.6.5  | PBI(Pd) MMMs solution preparation                            | 81 |
| 3.6.6  | Flat Sheet membrane casting for PBI membrane and PBI<br>MMMs | 81 |
| 3.7    | Characterization of Membrane                                 | 82 |
| 3.7.1  | Temperature programmed reduction (TPR) analysis              | 83 |
| 3.7.2  | X-ray diffraction (XRD) analysis                             | 83 |
| 3.7.3  | Fourier transform infrared (FTIR) Spectroscopy analysis      | 83 |
| 3.7.4  | Scanning electron microscope (SEM) analysis                  | 84 |
| 3.7.5  | Energy dispersive X-ray (EDX) analysis                       | 84 |
| 3.8    | Gas permeation test  | 84 |
| 3.8.1  | Gas permeation test for high operating temperature           | 87 |
| 3.8.2  | Single gas permeation test                                   | 88 |
| 3.8.3  | Mixed gas permeation test                                    | 89 |
| 3.9    | Van't Hoff Arrhenius equation                                | 90 |
| 3.10   | Polymath simulation for biohydrogen purification application | 90 |
| 3.10.1 | Membrane process simulation                                  | 91 |

## **CHAPTER FOUR: RESULTS AND DISCUSION**

|            |   |     |
|------------|---|-----|
| 4.1        | Characterization of Pd nanoparticles and PSf(Pd) MMMs | 97  |
| 4.1.1      | PSf(Pd/PEG) MMMs characterization                     | 97  |
| 4.1.1.1    | Characterization of Pd nanoparticles for Pd/PEG       | 97  |
| 4.1.1.1(a) | TEM analysis for Pd/PEG                               | 97  |
| 4.1.1.1(b) | XRD analysis for Pd/PEG                               | 98  |
| 4.1.1.2    | Characterization of PSf(Pd/PEG) MMMs                  | 99  |
| 4.1.1.2(a) | TPR analysis for Pd/PEG and<br>PSf(Pd/PEG) MMMs       | 99  |
| 4.1.1.2(b) | FTIR analysis for PSf(Pd/PEG) MMMs                    | 100 |
| 4.1.1.2(c) | SEM analysis for PSf(Pd/PEG) MMMs                     | 102 |
| 4.1.1.2(d) | EDX analysis for PSf(Pd/PEG) MMMs                     | 106 |
| 4.1.2      | PSf(Pd/PVP) MMMs characterization                     | 108 |
| 4.1.2.1    | Characterization of Pd nanoparticles for Pd/PVP       | 108 |
| 4.1.2.1(a) | TEM analysis for Pd/PVP                               | 108 |
| 4.1.2.1(b) | XRD analysis for Pd/PVP                               | 109 |
| 4.1.2.2    | Characterization of PSf(Pd/PVP) MMMs                  | 110 |
| 4.1.2.2(a) | TPR analysis for Pd/PVP and<br>PSf(Pd/PVP) MMMs       | 110 |
| 4.1.2.2(b) | FTIR analysis for PSf(Pd/PVP) MMMs                    | 112 |
| 4.1.2.2(c) | SEM analysis for PSf(Pd/PVP) MMMs                     | 113 |
| 4.1.2.2(d) | EDX analysis for PSf(Pd/PVP) MMMs                     | 116 |
| 4.2        | Gas separation performance of PSf(Pd) MMMs            | 117 |
| 4.2.1      | Performance analysis of PSf(Pd/PEG) MMMs              | 117 |
| 4.2.2      | Performance analysis of PSf(Pd/PVP) MMMs              | 121 |
| 4.3        | Characterization of Pd nanoparticles and PBI(Pd) MMMs | 125 |



|            |  |     |
|------------|--|-----|
| 4.3.1      | Characterization of PBI (Pd/PEG) MMMs (Low temperature permeation test)  | 125 |
| 4.3.1.1    | Characterization of PBI(Pd/PEG) MMMs                                     | 126 |
| 4.3.1.1(a) | XRD analysis for PBI(Pd/PEG) MMMs  | 126 |
| 4.3.1.1(b) | FTIR analysis for PBI(Pd/PEG) MMMs                                       | 126 |
| 4.3.1.1(c) | SEM analysis for PBI(Pd/PEG) MMMs  | 129 |
| 4.3.1.1(d) | EDX analysis for PBI(Pd/PEG) MMMs  | 132 |
| 4.3.2      | Characterization of PBI (Pd/PEG) MMMs (High temperature permeation test) | 132 |
| 4.3.2.1    | Characterization of Pd nanoparticles for Pd/PEG                          | 132 |
| 4.3.2.1(a) | TEM analysis for Pd/PEG  | 134 |
| 4.3.2.2    | Characterization of PBI(Pd/PEG) MMMs                                     | 134 |
| 4.3.2.2(a) | TPR analysis for Pd/PEG and PBI(Pd/PEG) MMMs                             | 134 |
| 4.3.2.2(b) | XRD analysis for PBI(Pd/PEG) MMMs  | 136 |
| 4.3.2.2(c) | FTIR analysis for PBI(Pd/PEG) MMMs                                       | 137 |
| 4.3.2.2(d) | SEM analysis for PBI(Pd/PEG) MMMs  | 139 |
| 4.3.2.2(e) | EDX analysis for PBI(Pd/PEG) MMMs  | 139 |
| 4.3.3      | Characterization of PBI (Pd/PVP) MMMs (High temperature permeation test) | 143 |
| 4.3.3.1    | Characterization of Pd nanoparticles for Pd/PVP                          | 143 |
| 4.3.3.1(a) | TEM analysis for Pd/PVP  | 143 |
| 4.3.3.2    | Characterization of PBI(Pd/PVP) MMMs                                     | 143 |
| 4.3.3.2(a) | TPR analysis for Pd/PVP and PBI(Pd/PVP) MMMs                             | 143 |

|  |     |
|--|-----|
| 4.3.3.2(b) XRD analysis for PBI(Pd/PVP) MMMs   | 144 |
| 4.3.3.2(c) FTIR analysis for PBI(Pd/PVP) MMMs  | 146 |
| 4.3.3.2(d) SEM analysis for PBI(Pd/PVP) MMMs   | 148 |
| 4.3.3.2(e) EDX analysis for PBI(Pd/PVP) MMMs   | 150 |
| 4.4 Gas performance for PBI(Pd) MMMs   | 151 |
| 4.4.1 Performance analysis of PBI(Pd/PEG) MMMs (Low temperature permeation test)   | 151 |
| 4.4.1.1 Comparison with literatures  | 154 |
| 4.4.2 Performance analysis of PBI(Pd/PEG) MMMs (High temperature permeation test)  | 154 |
| 4.4.2.1 Comparison with literatures  | 158 |
| 4.4.3 Performance analysis of PBI(Pd/PVP) MMMs (High temperature permeation test)  | 160 |
| 4.4.3.1 Single gas permeation  | 160 |
| 4.4.3.2 Mixed gas permeation   | 162 |
| 4.4.3.3 The effect of temperature on gas separation  | 164 |
| 4.4.3.4 Comparison with literatures  | 168 |
| 4.4.3.5 Comparison on the better performance of membrane in this work  | 170 |
| 4.4.3.6 Feasibility study on H <sub>2</sub> purification using PBI(Pd/PVP) membrane  | 172 |
| 4.4.3.6(a) Verification of mathematical model  | 172 |
| 4.4.3.6(b) Feasibility study of PBI(Pd/PVP)_1 membrane in H <sub>2</sub> purification for fermentation and gasification system | 173 |

## **CHAPTER FIVE: CONCLUSIONS AND RECOMMENDATIONS**

5.1 Conclusions 179

5.2 Recommendations 182

**REFERENCES** 183

## **APPENDICES**

Appendix A : Calculation of data analysis

Appendix B : Report of polymath simulation for Van't Hoff Arrhenius  
equation

Appendix C : Result of Gas Chromatography

Appendix D : Report of polymath simulation for membrane area and  
purity calculation

## **LIST OF PUBLICATIONS AND CONFERENCES**

## LIST OF TABLES

|   | <b>Page</b> |
|---|-------------|
| Table 1.1 Typical composition of gases from various processes (Liew et al., 2013).  | 10          |
| Table 1.2 The performance comparison of H <sub>2</sub> separation by different separation processes (Market, 2013).   | 14          |
| Table 2.1 Selected physical properties of H <sub>2</sub> , N <sub>2</sub> and CO <sub>2</sub> (Robeson et al., 2014).   | 28          |
| Table 2.2 The representative H <sub>2</sub> , N <sub>2</sub> , and CO <sub>2</sub> transport properties of H <sub>2</sub> selective membrane (commercial polymers). | 32          |
| Table 2.3 H <sub>2</sub> permeability of Pd and miscellaneous Pd alloys (wt%) at 350 °C (Al-Mufachi et al., 2015).  | 40          |
| Table 2.4 Microporous membrane for hydrogen separation  | 48          |
| Table 2.5 H <sub>2</sub> separation performance of MMMs reported in recent literatures.   | 54          |
| Table 2.6 Table summarizing the effect of stabilizer, filler loading and operating temperature on MMMs properties and performance.                                  | 62          |
| Table 2.7 Studies on the separation of biohydrogen using polymeric membranes(Ramírez-Morales et al., 2015).   | 64          |
| Table 3.1 List of chemical, reagents and gases used.  | 74          |
| Table 3.2 Pd nanoparticles loading in fabricated PSf membrane and PSf MMMs.   | 80          |

|           |  |     |
|-----------|--|-----|
| Table 3.3 | Pd nanoparticles loading in fabricated PBI MMMs samples.   | 82  |
| Table 3.4 | Specification of feed gas.   | 91  |
| Table 4.1 | Pure gas performance of MMMs with different Pd nanoparticles loadings at ambient temperature and pressure 1 bar.   | 118 |
| Table 4.2 | Pure gas permeabilities and pure gas selectivities of all membrane samples at ambient temperature and pressure at 1 bar.   | 122 |
| Table 4.3 | Pd nanoparticles loading in membrane samples and average membrane thickness estimated from SEM images.   | 132 |
| Table 4.4 | The weight percentage of stabilizer and Pd nanoparticles in PBI and PBI(Pd) MMMs and the thickness of membrane.  | 148 |
| Table 4.5 | Pure gas permeation/flux and pure gas gas selectivities of PBI and PBI(Pd) MMMs containing different Pd nanoparticles loading at 35 °C and and pressure at 3 bar.                  | 153 |
| Table 4.6 | Pure gas permeation/flux and pure gas gas selectivities of PBI and PBI(Pd) MMMs containing different Pd nanoparticles loading at pressure 5 bar and temperature 150 °C and 200 °C. | 156 |
| Table 4.7 | Pure gas permeability and pure gas gas selectivities of PBI and PBI MMMs containing different Pd   | 161 |

|            |   |     |
|------------|---|-----|
|            | nanoparticles loading at at operating temperature lower than 200 °C and pressure 5 bar.   |     |
| Table 4.8  | Pure gas permeability and pure gas gas selectivities of PBI(Pd/PVP)_1 at operating temperature higher than 200 °C and at pressure 5 bar.  | 166 |
| Table 4.9  | $E_p$ , $P_o$ and $R^2$ values of H <sub>2</sub> , N <sub>2</sub> and CO <sub>2</sub> in PBI(Pd/PVP)_1 determined using the Van't Hoff equation for operating temperature higher than 200 °C. | 168 |
| Table 4.10 | Pure gas permeability and pure gas selectivity of the better performance of membranes in this work  | 171 |

## LIST OF FIGURES

|  | <b>Page</b> |
|--|-------------|
| Figure 1.1 H <sub>2</sub> consumption worldwide in 2014 (Inc, 2015).   | 2           |
| Figure 1.2 H <sub>2</sub> ecosystem (Markets, 2016).   | 3           |
| Figure 1.3 Different conversion routes of biomass into H <sub>2</sub> (Mohanty et al., 2015).  | 8           |
| Figure 1.4 Upper bound correlation fo H <sub>2</sub> /N <sub>2</sub> and separation H <sub>2</sub> /CO <sub>2</sub> (Robeson, 2008). | 13          |
| Figure 2.1 Ideal concept of membrane separation technology (Li et al., 2015b).   | 26          |
| Figure 2.2 Schematic diagrams of gas transport mechanism gas separation membranes (Li et al., 2015b).                                | 28          |
| Figure 2.2 The chemical structure of PSf (Ismail et al., 2003).  | 33          |
| Figure 2.4 The chemical structure of PBI (Choi et al., 2015).  | 35          |
| Figure 3.1 Flow diagram of research methodology.   | 73          |
| Figure 3.2 Schematic diagram Pd synthesis preparation and membrane preparation.  | 75          |
| Figure 3.3 Schematic diagram of gas permeation test system.  | 85          |
| Figure 3.4 Gas permeation setup and membrane module  | 87          |
| Figure 3.5 Process flow for membrane module design (Geankoplis, 2003).   | 92          |
| Figure 3.6 Schematic diagram of single-stage membrane system.  | 95          |
| Figure 4.1 TEM image of synthesis Pd nanoparticles stabilized by PEG from inversed microemulsion method.                             | 98          |

|            |  |     |
|------------|--|-----|
| Figure 4.2 | X-ray diffraction patterns of Pd/PEG.  | 99  |
| Figure 4.3 | TPR profile of Pd/PEG and PSf(Pd/PEG)_3.   | 100 |
| Figure 4.4 | FTIR spectra of MMMs with Pd nanoparticles of (a) PSf, (b) PSf(PEG)_3, (c) PSf(PEG/MdCl)_3, (d) PSf(Pd/PEG)_1, (e) PSf(Pd/PEG)_3 and (f) PSf(Pd/PEG)_4.  | 101 |
| Figure 4.5 | SEM surface view images for (a) PSf, (b) PSf(PEG)_3, (c) PSf(PEG/MdCl)_3 and (d) PSf(Pd/PEG)_1, (e) PSf(Pd/PEG)_3, and (f) PSf(Pd/PEG)_4 membrane at magnification scale of 60 000×.   | 103 |
| Figure 4.6 | SEM cross section surface view images for (a) PSf upper layer, (b) PSf overall layer, (c) PSf(PEG)_3 upper layer, (d) PSf(PEG)_3 overall layer, (e) PSf(PEG/MdCl)_3 upper layer, and (f) PSf(PEG/MdCl)_3 overall layer of membrane at magnification scale of 15 000× for upper layer and 2 000× for overall layer.                       | 104 |
| Figure 4.7 | SEM cross section surface view images for (a) PSf(Pd/PEG)_1 upper layer, (b) PSf(Pd/PEG)_1 overall layer, (c) PSf(Pd/PEG)_3 upper layer, (d) PSf(Pd/PEG)_3 overall layer, (e) PSf(Pd/PEG)_4 upper layer, and (f) PSf(Pd/PEG)_4 overall layer of membrane at magnification scale of 15 000× for upper layer and 2 000× for overall layer. | 105 |
| Figure 4.8 | The EDX line analysis along arrow line from top to bottom of Pd nanoparticles entrapped PSf membrane (a)   | 107 |



|             |   |     |
|-------------|---|-----|
|             | PSf(Pd/PEG)_1 (purple shift), (b) PSf(Pd/PEG)_3 (pink shift) and (c) PSf(Pd/PEG)_4 (red shift).   |     |
| Figure 4.9  | TEM image of synthesis Pd nanoparticles stabilized by PVP in inversed microemulsion.  | 109 |
| Figure 4.10 | X-ray diffraction patterns for crystalline Pd nanoparticles stabilized by PVP.  | 110 |
| Figure 4.11 | TPR profile for Pd/PVP and PSf(Pd/PVP)_2.   | 111 |
| Figure 4.12 | FTIR patterns of of (a) PSf, (b) PSf(Pd/PVP)_1, (c) PSf(Pd/PVP)_2, and (d) PSf(Pd/PVP)_3 of MMMs samples.   | 113 |
| Figure 4.13 | SEM images on the surface of (a) PSf, (b) PSf(Pd/PVP)_1, (c) PSf(Pd/PVP)_2, and (d) PSf(Pd/PVP)_3 of MMMs samples at magnification scale of 16 000×.      | 115 |
| Figure 4.14 | SEM images on the cross-section of (a) PSf, (b) PSf(Pd/PVP)_1, (c) PSf(Pd/PVP)_2, and (d) PSf(Pd/PVP)_3 of MMMs samples at magnification scale of 2 000×. | 116 |
| Figure 4.15 | EDX results for (a) 1 wt.% Pd and (b) 3 wt.% PSf(Pd) MMMs showing the concentration of Pd element across a cross sectional line of the membranes.         | 117 |
| Figure 4.16 | Comparison of recent literatures with PSf membranes prepared for H <sub>2</sub> /N <sub>2</sub> gas pair.   | 124 |
| Figure 4.17 | Comparison of recent literatures with PSf of membranes prepared for H <sub>2</sub> /CO <sub>2</sub> gas pair.   | 125 |

|             |   |     |
|-------------|---|-----|
| Figure 4.18 | X-ray diffraction patterns for (a) PBI(Pd/PEG)_1 and (b) PBI(Pd/PEG)_4 MMMs.  | 127 |
| Figure 4.19 | FTIR spectra for (a) PBI, (b) PBI(Pd/PEG)_1 and (c) PBI(Pd/PEG)_4 MMMs.   | 128 |
| Figure 4.20 | SEM surface view images for (a) PBI (b) PBI(Pd/PEG)_1 and (c) PBI(Pd/PEG)_4 membrane at magnification scale of 10 000×.                         | 130 |
| Figure 4.21 | SEM cross section surface view images for (a) PBI (b) PBI(Pd/PEG)_1 and (c) PBI(Pd/PEG)_4 membrane at magnification scale of 20 000×.           | 131 |
| Figure 4.22 | EDX line analysis along arrow line from top to bottom of (a) PBI, (b) PBI(Pd/PEG)_1 MMM (pink shift) and (c) PBI(Pd/PEG)_4 MMMs (purple shift). | 133 |
| Figure 4.23 | TEM image of Pd/PEG nanoparticles in inversed microemulsion method.   | 135 |
| Figure 4.24 | TPR profile of Pd/PEG and PBI(Pd/PEG)_2.  | 135 |
| Figure 4.25 | XRD patterns for (a) PBI(Pd/PEG)_2, (b) PBI(Pd/PEG)_3 and (c) PBI(Pd/PEG)_4 MMMs.   | 137 |
| Figure 4.26 | FTIR spectra for (a) PBI, (b) PBI(Pd/PEG)_2, (c) PBI(Pd/PEG)_3 and (d) PBI(Pd/PEG)_4 MMMs.  | 138 |
| Figure 4.27 | SEM surface view images for (a) PBI, (b) PBI(Pd/PEG)_2, (c) PBI(Pd/PEG)_3 and (d) PBI(Pd/PEG)_4 MMMs at magnification scale of 5 000×.          | 140 |
| Figure 4.28 | SEM cross section view images for (a) PBI, (b) PBI(Pd/PEG)_2, (c) PBI(Pd/PEG)_3 and (d)   | 141 |

|             |   |     |
|-------------|---|-----|
|             | PBI(Pd/PEG)_4 MMMs at magnification scale of 5 000×.  |     |
| Figure 4.29 | EDX line analysis along arrow line from top to bottom of (a) PBI(Pd/PEG)_2 (purple shift), (b) PBI(Pd/PEG)_3 (red shift) and (c) PBI(Pd/PEG)_4 MMMs (purple shift). | 142 |
| Figure 4.30 | TEM image of Pd/PVP nanoparticles.  | 144 |
| Figure 4.31 | TPR profile of (a) Pd/PVP, (b) PBI(Pd/PVP)_1 and (c) PBI(Pd/PVP)_3 membrane.  | 145 |
| Figure 4.32 | X-ray diffraction pattern of (a) PBI(Pd/PVP)_1 (red line) and (b) PBI(Pd/PVP)_3 membrane (blue line).   | 146 |
| Figure 4.33 | FTIR spectra of (a) PBI, (b) PBI(PVP)_1, (c) PBI(Pd/PVP)_1 and (d) PBI(Pd/PVP)_3 membrane.  | 147 |
| Figure 4.34 | SEM surface view images for (a) PBI, (b) PBI(PVP)_1, (c) PBI(Pd/PVP)_1 and (d) PBI(Pd/PVP)_3 membrane at magnification scale of 10 000×.                            | 149 |
| Figure 4.35 | SEM cross section surface view images for (a) PBI, (b) PBI(PVP)_1, (c) PBI(Pd/PVP)_1 and (d) PBI(Pd/PVP)_3 membrane at magnification scale of 5 000×.               | 150 |
| Figure 4.36 | The EDX result of Pd nanoparticles entrapped PBI membrane (a) PBI(Pd/PVP)_1 and (b) PBI(Pd/PVP)_3 membrane.   | 151 |
| Figure 4.37 | H <sub>2</sub> /CO <sub>2</sub> separation performance of PBI(Pd/PEG)_1 membrane compared to the Robeson upper bound at 35 °C.                                      | 155 |
| Figure 4.38 | The comparison of the PBI(Pd/PEG)_2 membrane with PBI MMMs reported in literature (30/70 (w/w) ZIF-8-PBI  | 159 |

(Yang and Chung, 2013a), 45/55 (w/w) ZIF-90-PBI (Yang and Chung, 2013b), 16.1 wt% ZIF-11-PBI (Li et al., 2014b), 50/50 (w/w) ZIF-7-PBI (Yang et al., 2011), 30/70 (w/w) ZIF-8-PBI (Yang et al., 2012) membranes and 20 wt% ZIF-8-PBI membranes (Sánchez-Laínez et al., 2016) on Robeson plot.

|             |  |     |
|-------------|--|-----|
| Figure 4.39 | The permeate composition in the H <sub>2</sub> separation from (a) H <sub>2</sub> -CO <sub>2</sub> mixture and (b) H <sub>2</sub> -N <sub>2</sub> mixture using PBI membrane and PBI(Pd/PVP) <sub>1</sub> MMMs at 200 °C.  | 163 |
| Figure 4.40 | Temperature dependence on gas permeability (P) in PBI(Pd/PVP) <sub>1</sub> membrane.   | 167 |
| Figure 4.41 | The comparison of H <sub>2</sub> /CO <sub>2</sub> separation performance of PBI(Pd/PVP) <sub>1</sub> membrane and PBI based membranes reported in literature using the Robeson upper plot.   | 169 |
| Figure 4.42 | The comparison between the permeate purity calculated in this work and the permeate purity calculated in other works (Wukovits et al., 2012, Lassmann et al., 2016).   | 173 |
| Figure 4.43 | The effects of temperature on the required membrane area of PBI(PVP/Pd) <sub>1</sub> membrane to recover 90 % H <sub>2</sub> from a mixture of H <sub>2</sub> and CO <sub>2</sub> (50 mol% : 50 mol%) for (a) fermentation system and (b) gasification system.     | 175 |
| Figure 4.44 | The effects of temperature on the predicted purity of H <sub>2</sub> of PBI(PVP/Pd) <sub>1</sub> membrane to recover 90 % H <sub>2</sub> from a mixture of H <sub>2</sub> and CO <sub>2</sub> (50 mol% : 50 mol%) for both system (fermentation and gasification). | 176 |

- Figure 4.45 The H<sub>2</sub> purity and recovery predicted using PBI(PVP/Pd)\_1 membrane at 300 °C for both system (fermentation and gasification). 177
- Figure 4.46 The predicted H<sub>2</sub> purity and the required membrane area separation performance of PBI(Pd/PVP)\_1 membrane and PBI based membranes reported in literature using the Robeson upper plot and their membrane area predicted by simulation result (recovery = 90 %) for (a) fermentation system and (b) gasification system. Note : The permeability and selectivity value of each membrane sample was taken from literature as stated in Figure. 177

## LIST OF ABBREVIATIONS

|                 |                               |
|-----------------|-------------------------------|
| Ag              | Argentum                      |
| Al              | Aluminium                     |
| AlPO            | Aluminophosphate              |
| APTES           | 3-Aminopropyltriethoxysilane  |
| ATR             | Attenuated total reflection   |
| Au              | Gold                          |
| B               | Boron                         |
| C               | Carbon                        |
| CA              | Cellulose acetate             |
| Ce              | Cerium                        |
| CH <sub>4</sub> | Methane                       |
| CMS             | Carbon molecular sieve        |
| CO              | Carbon monoxide               |
| CO <sub>2</sub> | Carbon dioxide                |
| Cu              | Copper                        |
| CVD/MOCVD       | Chemical vapor deposition     |
| DMAc            | <i>N,N</i> -dimethylacetamide |
| DOE             | Department of environment     |
| EDX             | Energy dispersive X-ray       |
| EG              | Ethylene glycol               |
| EP              | Electroless plating           |
| EtOH            | Ethanol                       |
| Fcc             | Face centered cubic           |
| FTIR            | Fourier transformed infrared  |

|                                  |   |
|----------------------------------|---|
| GC                               | Gas chromatography                                |
| Gd                               | Gadolinium  |
| GPU                              | Gas permeation unit                               |
| H                                | Hydrogen atom                                     |
| H <sub>2</sub>                   | Hydrogen gas                                      |
| H <sub>2</sub> O                 | Water   |
| H <sub>2</sub> PdCl <sub>4</sub> | Dihydrogentetrachloropalladate                    |
| H <sub>2</sub> S                 | Hydrogen sulphide                                 |
| HCl                              | Hydrochloric acid                                 |
| HDPE                             | High-density polyethylene                         |
| He                               | Helium  |
| HFA                              | 4,4'-(hexafluoro-isopropylidene)bis(benzoic acid) |
| HMA                              | 2-hydroxy 5-methyl aniline                        |
| HVOF                             | High velocity oxy-fuel spraying                   |
| IPA                              | Isopropyl alcohol                                 |
| LED                              | Light-emitting diode                              |
| LiCl                             | Lithium chloride                                  |
| MeOH                             | Methanol  |
| MdCl                             | Methane dichloride                                |
| MgO                              | Magnesium oxide                                   |
| MMMs                             | Mixed matrix membranes                            |
| MMMSCFD                          | Million standard cubic feet per day               |
| MOF                              | Metal organic framework                           |
| MSS                              | Molecular sieve silica                            |
| MWCNTs                           | Multi-walled carbon nanotubes                     |
| N <sub>2</sub>                   | Nitrogen  |

|                   |   |
|-------------------|---|
| NaOH              | Sodium hydroxide  |
| Ni                | Nickel  |
| O                 | Oxygen atom   |
| O <sub>2</sub>    | Oxygen  |
| PAMH              | Proton-exchanged AMH-3  |
| PBI               | Polybenzimidazole   |
| PBNPI             | Poly(bisphenol A-co-4-nitrophthalic anhydride-co-1,3-phenylene diamine) |
| PC                | Polycarbonate   |
| Pd                | Palladium   |
| PdAc <sub>2</sub> | Palladium acetate   |
| PdCl <sub>2</sub> | Palladium chloride  |
| PdH <sub>x</sub>  | Palladium hydride   |
| PDMS              | Polydimethylsiloxane  |
| PdO               | Palladium oxide   |
| PEG               | Polyethylene glycol   |
| PEI               | Polyetherimide  |
| PES               | Polyethersulfone  |
| PI                | Polyimide   |
| PILs              | Proton conducting ionic liquids   |
| PIM-1             | Polymers of intrinsic microporosity                                     |
| PMF               | Poly(melamine <i>co</i> -formaldehyde)                                  |
| PMP               | Polymethylpentene   |
| PPO               | Polyphenylene Oxide   |
| PSA               | Pressure swing adsorption   |
| PSf               | Polysulfone   |



|                  |                                   |
|------------------|-----------------------------------|
| PSf-Ac           | Polysulfone-acrylate              |
| PSS              | Porous stainless steel            |
| Pt               | Platinum                          |
| PVAc             | Polyvinyl acetate                 |
| PVC              | Polyvinyl chloride                |
| PVD              | Physical vapor deposition         |
| PVDF             | Polyvinylidene difluoride         |
| PVP              | Polyvinylpyrrolidone              |
| PVTMS            | Poly(vinyl trimethylsilane)       |
| PXDA             | <i>p</i> -Xylene diamine          |
| S                | Sulfur                            |
| SAPO             | Silicoaluminophosphate            |
| SEM              | Scanning electron microscope      |
| SMR              | Steam methane reforming           |
| SnO <sub>2</sub> | Stannic oxide                     |
| TCD              | Thermal conductive detector       |
| TEM              | Transmission electron micrographs |
| THF              | Tetrahydrofuran                   |
| TiO <sub>2</sub> | Titanium oxide                    |
| TPR              | Temperature programmed reduction  |
| TSA              | Temperature swing adsorption      |
| WGS              | Water-gas shift reaction          |
| XRD              | X-ray diffraction                 |
| ZIF              | Zeolite imidazolate framework     |
| Y                | Yttrium                           |
| Zr               | Zirconium                         |

## LIST OF SYMBOLS

|                    |   |
|--------------------|---|
| $A$                | Membrane effective surface area                       |
| $\dot{A}$          | Kinetic diameter                                      |
| $A_m$              | Membrane area   |
| $E_p$              | Apparent activation energy                            |
| $H_{2\text{ pty}}$ | Hydrogen purity                                       |
| $H_{2\text{ rcy}}$ | Hydrogen recovery                                     |
| $l$                | Membrane skin thickness                               |
| $n_{H_2 p}$        | Molar flow rate of hydrogen in permeate               |
| $n_i$              | Molar flow rate of component $i$                      |
| $n_{Tp}$           | Total molar flow rate                                 |
| $\theta$           | The cut or fraction of feed permeate                  |
| $p$                | Pressure  |
| $p_p$              | Total pressure in the low pressure (permeate) side    |
| $p_f$              | Total pressure in the high pressure (feed) side       |
| $\Delta p$         | Pressure difference across membrane                   |
| $p_i$              | Partial pressure of gas component $i$                 |
| $P$                | Pure gas permeability                                 |
| $P_i$              | Pure gas permeability of component $i$                |
| $P_i/l$            | Pure gas permeability of component $i$ over thickness |
| $P_o$              | Pre-exponential coefficients                          |
| $Q_i$              | Volumetric flow rate of gas component $i$             |
| $R$                | Gas constant  |
| $R^2$              | Regression analysis                                   |

|               |   |
|---------------|---|
| $T$           | Temperature   |
| $T_g$         | Glass transition temperature  |
| wt%           | Percentage by weight  |
| vol%          | Percentage by volume  |
| mol%          | Percentage by mol   |
| $\alpha_{ij}$ | Pure gas selectivity of component $i$ over component $j$                              |
| $i, j$        | Gas component H <sub>2</sub> and N <sub>2</sub> or H <sub>2</sub> and CO <sub>2</sub> |
| $f$           | Feed  |
| $r$           | Retentate   |
| $p$           | Permeate  |

# MEMBRAN MATRIKS CAMPURAN DIPERBADANKAN DENGAN PARTIKEL PALLADIUM UNTUK PEMISAHAN HIDROGEN

## ABSTRAK

Satu inovasi dalam pemilihan membran untuk hidrogen ( $H_2$ ) memegang kunci penting kepada ekonomi hidrogen. Polimer adalah bahan yang paling praktikal dan menjimatkan untuk fabrikasi membran, tetapi penggunaan membran polimer termasuk polysulfone (PSf) dan polybenzimidazole (PBI) membran untuk pemisahan  $H_2$  sentiasa terhad oleh "keseimbangan" antara pemilihan dan kebolehtelapan. Dalam kerja ini, nanopartikel Pd yang dimasukkan ke dalam membran PSf dan PBI mengatasi batasan tersebut. Sebelum pengadunan, nanopartikel Pd telah disintesis secara kinetik dan distabilkan dalam mikroemulsi songsang oleh polyethylene glycol (PEG) atau Polyvinylpyrrolidone (PVP). PSf membran matriks campuran (MMMs) telah disediakan melalui fasa penyongsangan kering-basah manakala MMMs PBI yang padat telah disintesis melalui fasa penyongsangan kering. Keputusan X-ray diffraction (XRD) dan Energy dispersive X-ray (EDX) mengesahkan kemasukan nanopartikel Pd telah berjaya. PSf(Pd/PEG)\_3 MMM menunjukkan prestasi pemilihan yang paling tinggi (pemilihan tulen  $H_2/N_2$  : 21.69, pemilihan tulen  $H_2/CO_2$  : 1.98 dan kebolehtelapan  $H_2$ : 161.84 Barrer) berbanding membran PSf yang dicampur dengan nanopartikel Pd dalam PEG yang lain. Penambahan PEG mendorong perubahan struktur seperti jari menjadi sel-sel tertutup dan pertumbuhan lapisan tebal. Kebolehtelapan  $H_2$  yang besar telah dicapai dengan menggunakan 2 % nanopartikel Pd dalam PVP untuk membran PSf. (pemilihan Ideal  $H_2/N_2$  : 20, pemilihan ideal  $H_2/CO_2$  : 6.2 dan kebolehtelapan  $H_2$  : 5781.07 Barrer). Peningkatan ini boleh dikaitkan dengan perubahan ruang kosong dalam polimer dan pertumbuhan lapisan padat yang disebabkan oleh PVP. Pada 200 °C, MMMs PBI dengan kestabilan haba yang luar biasa telah mencapai pemilihan  $H_2/CO_2$  dan  $H_2/N_2$  yang terbaik apabila 2 hingga 4 % nanopartikel Pd dalam PEG telah dimasukkan. Pemilihan  $H_2/CO_2$  oleh membran PBI(Pd/PEG)\_2 adalah 18.56 (kebolehtelapan  $H_2$  : 53.22 Barrer) manakala pemilihan  $H_2/N_2$  oleh membran PBI(Pd/PEG)\_4 adalah 108.28 (kebolehtelapan  $H_2$  : 62.40 Barrer). Pemilihan  $H_2$  yang lebih tinggi telah dicapai dengan menggunakan PVP sebagai penstabil dalam PBI(Pd) MMMs

berbanding PBI(Pd) MMMs dengan PEG. Membran PBI (Pd/PVP)\_1 dengan 1 % nanopartikel Pd dalam PVP mencapai pemilihan tulen H<sub>2</sub>/CO<sub>2</sub> iaitu 19.73 dan pemilihan tulen H<sub>2</sub>/N<sub>2</sub> iaitu 252.54 (kebolehtelapan H<sub>2</sub> : 32.41 Barrer). Kedua-dua membran PBI(Pd/PEG)\_2 dan PBI (Pd/PVP)\_1 melepasi had atas 'Robeson plot' dengan jayanya. Untuk membran PBI, pekali resapan bergantung kuat kepada suhu dengan sumbangan minimum oleh kelarutan dalam pemilihan gas dan kebolehtelapan. Tenaga pengaktifan dikurangkan dengan banyak oleh PBI MMMs dan ia boleh menandakan pengurangan penyebaran gas disebabkan oleh pengurangan dalam ruang kosong. Walau bagaimanapun, keutamaan penyerapan oleh H<sub>2</sub> dalam semua MMMs dengan nanopartikel Pd boleh berkaitan dengan interaksi antara H-Pd. Walaupun tingkah laku penyerapan berbeza antara gas tulen dan campuran disebabkan oleh tingkah laku pengangkutan, PBI(Pd/PVP)\_1 MMMs telah menunjukkan peningkatan yang mengagumkan oleh H<sub>2</sub> di pengeluaran berbanding dengan membran PBI yang asal untuk nisbah 50/50. Ketulenan 98.7 % H<sub>2</sub> dicapai pada 90 % pemulihan H<sub>2</sub>. Dalam kajian ini, pemuatan nanopartikel Pd dan suhu operasi memberi kesan kepada ketulenan dan pemulihan H<sub>2</sub> disebabkan perubahan pada kebolehtelapan dan pemilihan membran.

# MIXED MATRIX MEMBRANES INCORPORATED WITH PALLADIUM NANOPARTICLES FOR HYDROGEN SEPARATION

## ABSTRACT

An innovation in hydrogen ( $H_2$ ) selective membrane holds the important key to hydrogen economy. Polymers are the most practical and economical material for membrane fabrication, but the application of polymeric membranes including polysulfone (PSf) and polybenzimidazole (PBI) membranes in  $H_2$  separation is always limited by the “trade-off” between selectivity and permeability. In this work, Pd nanoparticles are incorporated into PSf and PBI membranes to overcome the mentioned limitations. Before blending, Pd nanoparticles were kinetically synthesized and stabilized in the inversed microemulsion of polyethylene glycol (PEG) or polyvinylpyrrolidone (PVP). The PSf mixed matrix membranes (MMMs) were prepared by dry-wet phase inversion while the dense PBI MMMs were synthesized by dry phase inversion. The X-ray diffraction (XRD) and Energy dispersive X-ray (EDX) results confirmed that the Pd nanoparticles incorporation was successful. The PSf(PEG/Pd)\_3 MMM showed the highest separation performance (pure gas  $H_2/N_2$  selectivity : 21.69, pure gas  $H_2/CO_2$  selectivity: 1.98 and  $H_2$  permeability : 161.84 Barrer) among the PSf membranes blended with Pd nanoparticles in PEG. The addition of PEG induced the changes of finger-like structure into closed cells and the growth of dense layer. High  $H_2$  permeability was achieved using 2 wt% of Pd nanoparticles loading in PVP for PSf membrane (pure gas  $H_2/N_2$  selectivity : 20, pure gas  $H_2/CO_2$  selectivity : 6.2 and  $H_2$  permeability : 5781.07 Barrer). The improvement could be related to the changes of free volume in polymer and the growth of dense layer caused by PVP. At 200°C, PBI MMMs with remarkable thermal stability achieved excellent  $H_2/CO_2$  and  $H_2/N_2$  selectivities when 2 to 4 wt% of Pd nanoparticles in PEG were incorporated. The  $H_2/CO_2$  selectivity of PBI(Pd/PEG)\_2 membrane was 18.56 ( $H_2$  permeability : 53.22 Barrer) while the  $H_2/N_2$  selectivity of PBI(Pd/PEG)\_4 membrane was 108.28 ( $H_2$  permeability: 62.40 Barrer). A higher selectivity of  $H_2$  was achieved by using PVP as the stabilizer in PBI(Pd) MMMs in comparison to the PBI(Pd) MMMs with PEG. The PBI(Pd/PVP)\_1 membrane with 1 wt% of Pd nanoparticles loading in PVP achieved

a pure gas H<sub>2</sub>/CO<sub>2</sub> selectivity of 19.73 and a pure gas H<sub>2</sub>/N<sub>2</sub> selectivity of 252.54 (H<sub>2</sub> permeability : 32.41 Barrer). Both PBI(Pd/PEG)\_2 and PBI(Pd/PVP)\_1 membranes surpass the upper bound of Robeson plot successfully. For PBI membranes, the diffusion coefficients depend on temperature strongly with minimal contribution of solubility into gas selectivity and permeability. The activation energy reduced greatly in PBI MMMs and it could signify the reduction of gas diffusion due to a drop in free volume. However, the preferential sorption of H<sub>2</sub> in all MMMs with Pd nanoparticles could be related to the H-Pd interaction. Eventhough the permeation behavior is different between pure and mixed gas permeation due to their transport behavior, the PBI(Pd/PVP)\_1 MMMs for mixed gas showed an impressive improvement of H<sub>2</sub> in permeate compare to neat PBI membrane for 50/50 ratio. The 98.7 % H<sub>2</sub> purity was achieved at 90 % H<sub>2</sub> recovery. In this study, Pd nanoparticles loading and operating temperature gave significance effect on purity and recovery of H<sub>2</sub> due to the changes on permeability and selectivity of membrane.

## CHAPTER ONE

### INTRODUCTION

#### 1.1 Hydrogen Demand and Production

Hydrogen (H<sub>2</sub>) is a valuable commodity which has been widely considered to be an attractive energy carrier and storage medium with high gravimetric energy density ( $1.43 \times 10^8$  J/Kg) (Li et al., 2015). The demand for H<sub>2</sub> in fertilizer production, petroleum industry, fuel cell, transportation, energy storage and other applications is expected to increase from 168 million kg in 2013 to nearly 3.5 billion kg in 2030 (Martin, 2014). The demand is predicted to grow due to the strict regulatory norms to desulfurize petroleum products and search for a clean fuel option. H<sub>2</sub> is carbon free fuel and water is the only by-product. H<sub>2</sub> can be produced by the electrolysis of water using renewable energies such as wind, solar and water instead of the conventional production routes such as steam methane reforming, partial oxidation of oil and coal gasification. Biohydrogen can be also produced using photobiological systems, dark fermentation systems or hybrid systems (Bharathiraja et al., 2016).

The fertilizers and petroleum industries are the largest H<sub>2</sub> users at the moment, consuming 50 % and 37 % of the total H<sub>2</sub> produced respectively (Bharathiraja et al., 2016). In 2014, Asia pacific became the largest market for H<sub>2</sub> consumption as shown in Figure 1.1 due to the growing demand for petroleum products from refineries with lower sulphur content. China is expected to consume a great amount of H<sub>2</sub> for fuel cell electric vehicles by enacting clean fuel regulations to achieve carbon emission target. Europe held the second largest market share



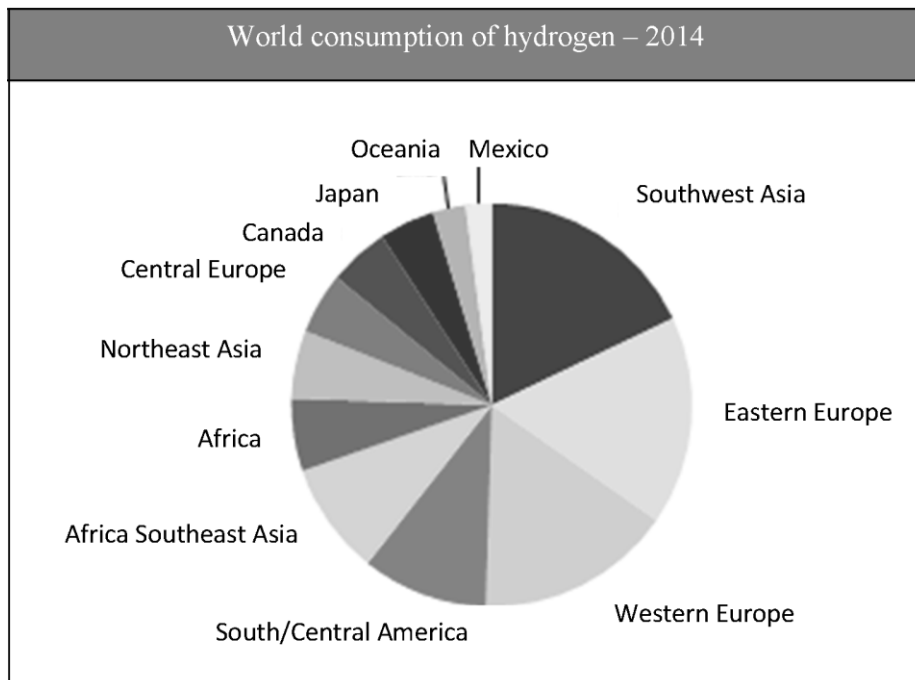


**Figure 1.1:** H<sub>2</sub> consumption worldwide in 2014 (Inc, 2015).

followed by North America. However, the H<sub>2</sub> demand of North America is expected to grow faster than the H<sub>2</sub> demand of Europe owing to the increased shale gas exploration (Research, 2016).

The supply chain of the H<sub>2</sub> starts from the primary energy sources which are further utilized for various generation, and application purposes as illustrated in Figure 1.2. The H<sub>2</sub> production plants can utilize the produced H<sub>2</sub> or further distribute H<sub>2</sub> to other market player for various applications. Some of the leading players in the H<sub>2</sub> market include Linde AG (Germany), Air Liquide SA (France), Air Products & Chemicals Inc. (U.S.), Praxair Inc. (U.S.), Airgas Inc. (U.S), and Hydrogenics Corp. (Canada).

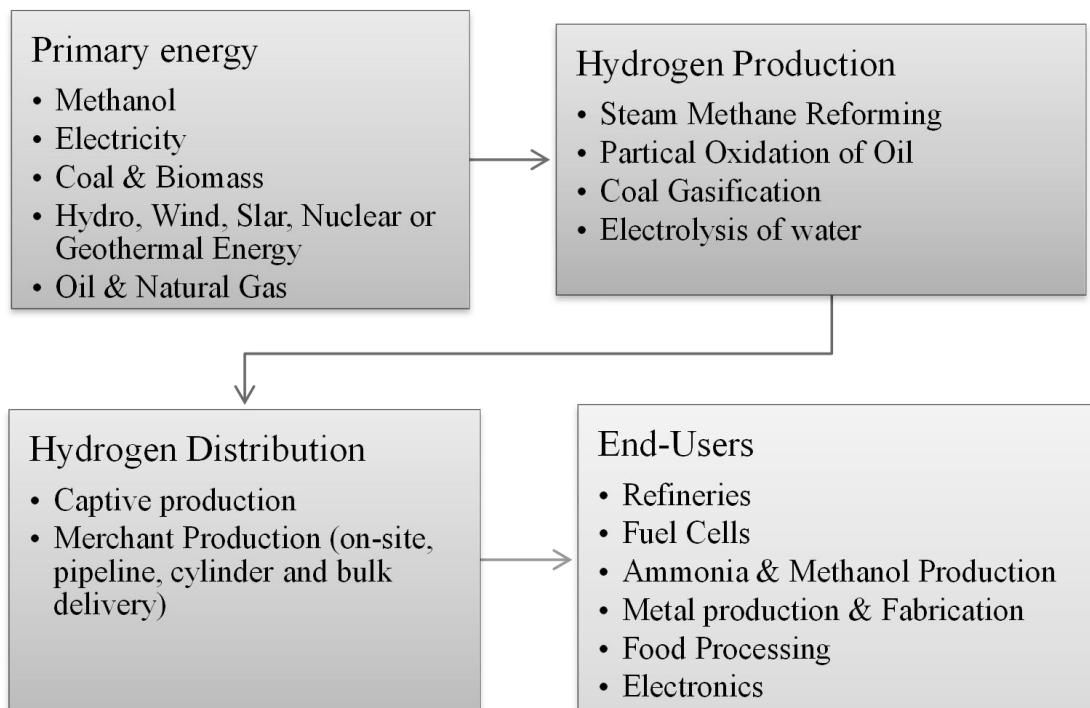
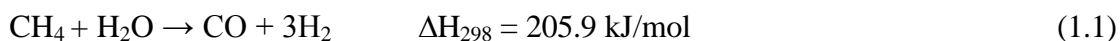
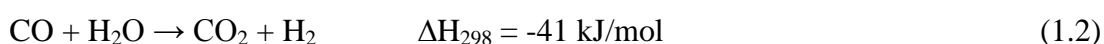


**Figure 1.2:** H<sub>2</sub> ecosystem (Markets, 2016).

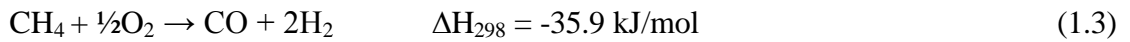
Currently, around 49 % of the global H<sub>2</sub> demand is met by steam reforming using natural gas. Oil reforming contributes 29 % of the total H<sub>2</sub> generation while coal gasification contributes another 18 % of the total H<sub>2</sub> production (Inc, 2015). The remaining H<sub>2</sub> is produced from water electrolysis (3.9 %) and other sources (0.1 %) (Kalamaras and Efstathio, 2013). The dominant route for H<sub>2</sub> production at industrial scale involves the steam reforming of natural gas followed by gas purification. The common efficiency of steam reforming is 80 %. The production of H<sub>2</sub> by steam methane reforming (SMR) at a distributed scale is projected to be more cost effective compared to the central production of H<sub>2</sub> at large scale with delivery via compressed gas tube trailers or cryogenic trucks (Gupta, 2008). Steam reforming is typically conducted within a temperature range of 700 to 1000 °C and a pressure range of 3 to 25 bar. The reaction for SMR is shown in equation 1.1 (Liu et al., 2010).



Besides H<sub>2</sub>, the reaction also produces about 12 % of carbon monoxide (CO), which can be further converted into carbon dioxide (CO<sub>2</sub>) and H<sub>2</sub> through the water-gas shift reaction (WGS). For instance, the SMR plant in Pasadena, Texas produces H<sub>2</sub> at a rate of 80 million standard cubic feet per day (MMMSCFD) using the steam reforming and WGS reactions followed by pressure swing absorption to remove the remaining traces of CO, CO<sub>2</sub>, steam and methane (CH<sub>4</sub>) from H<sub>2</sub> (Reformer, 2013). In the small and large SMR plants, natural gas feedstock cost contributes up to 68 % of the final H<sub>2</sub> price and the remaining expenses compose of capital charges. According to Muradov and Veziroglu (2005), a typical H<sub>2</sub> plant with a production capacity of 1 million m<sup>3</sup> H<sub>2</sub>/day releases around 0.3 - 0.4 million m<sup>3</sup> of CO<sub>2</sub> daily depending on the separation processes. The capture of CO<sub>2</sub> may induce additional cost, approximately 25 - 30 % (Hoseini and Wahid, 2016). The CO<sub>2</sub> and H<sub>2</sub> gases are produced according to the following stoichiometries (Liu et al., 2010);



In partial oxidation, natural gas and oxygen (O<sub>2</sub>) are introduced into a reactor at high pressure (15 - 30 atm). An exothermic oxidation reaction is initiated to form H<sub>2</sub> and CO. Similar to SMR, the formation of H<sub>2</sub> from CO is further accomplished via WGS. The use of catalyst can reduce the reaction temperature to 800 - 900 °C in catalytic partial oxidation. Equation 1.3 below shows the relevant stoichiometric equation for partial oxidation reaction (Liu et al., 2010).



Since the reaction is exothermic, no external heat supply is necessary and the capital cost is reduced. SMR and partial methane oxidation are well developed processes, the cost of H<sub>2</sub> production depend on the cost of natural gas greatly (Paul, 2014). Autothermal reforming further combines SMR and partial methane oxidation to achieve exothermic state with outlet temperature in the range of 950 to 1100 °C and pressure as high as 100 bar. WGS is required to convert CO into H<sub>2</sub>, but the efficiency of autothermal reforming is limited by the gas purification step (Riis et al., 2006).

The partial oxidation of oil is another major route of H<sub>2</sub> production and it has been widely commercialized. Several modifications are required based on the feed composition and the reactor type. The catalytic or noncatalytic partial oxidation processes are exothermic due to the sufficient amount of oxygen added. The noncatalytic partial oxidation of heavy oil is conducted at high temperature (1100 - 1500 °C) while the catalytic partial oxidation of light hydrocarbon such as naphtha can be conducted at a lower temperature (600 - 900 °C) (Gupta, 2008). The syngas is shifted, desulfurized and methanated.

The H<sub>2</sub> production from coal gasification is also well-established, but it is only competitive with SMR when oil and gas price is high (Padró and Putsche, 1999). In coal gasification, the process involves the partial oxidation of coal using O<sub>2</sub> followed by steam reforming in a high pressure reactor. Two types of coal gasification processes are commercially used, name Koppers-Totzek process and

Texaco process. The Koppers-Totzek process is operated at atmospheric pressure while the Texaco process is operated at a pressure of 5.5 MPa. The syngas is then desulfurized, shifted and purified subsequently. Both processes result in H<sub>2</sub> product streams with purities of at least 97 % (Mirabal, 2003).

Although H<sub>2</sub> is considered a clean energy, 98 % of H<sub>2</sub> actually generated from fossil fuel as discussed earlier. At the present rate of fossil fuel consumption, the reserves are predicted to be finished in less than 50 years (Mclamb, 2011). The dependence on fossil fuels not only contributes climate change and global warming, but also causes a rapid exhaustion of natural energy sources. Hence, H<sub>2</sub> should be produced from clean and abundant resources using environmentally benign methods. Rohland et al., (1992) predicted that the renewable resources will meet 36 % of the total global energy demand by 2025, with H<sub>2</sub> contribution of 11 %. If the H<sub>2</sub> production technology is further improved, the use of coal and crude oil will drop to 36.7 % and 40.5 % respectively, by 2030.

H<sub>2</sub> can be generated from water and electricity through electrolysis, the reverse of the process used in a fuel cell. Water electrolysis has been extensively developed in recent years and supplying up to 4 % of current total H<sub>2</sub> production (Gupta, 2008). Water electrolysis is an electrochemical reaction which yields H<sub>2</sub> and O<sub>2</sub> and the charge carrier can be OH<sup>-</sup>, H<sub>3</sub>O<sup>+</sup> or O<sup>2-</sup>. Alkaline electrolysis is a mature technology for H<sub>2</sub> production a large scale, but it only offers low current density and the system is highly corrosive. Polymer electrolyte membrane electrolysis with high power density is also commercially available at expensive price besides alkaline electrolysis. Furthermore, solid oxide electrolysis has been recently developed to

achieve high electrical efficiency (Götz et al., 2016). Water can be further electrolyzed using solar or wind energy to produce H<sub>2</sub> with minimum environmental impacts. However, the H<sub>2</sub> produced using water electrolysis is estimated to be much more expensive than the non-renewable H<sub>2</sub> discussed earlier (Gandía et al., 2013). The electrolysis usually loses 10 - 30 % of the input energy and 39 kWh of electricity is required to produce 1 kg of H<sub>2</sub> even 100 % efficiency is achieved (Gardner, 2009).

Through biomass conversion processes, H<sub>2</sub>-containing gas can be produced similarly to coal gasification. The biomass particles undergo partial oxidation, resulting in gas and charcoal production at the temperature higher than 1000 K (Ni et al., 2006). Biomass gasification is categorized as thermochemical conversion which is the most widely practiced conversion pathway for H<sub>2</sub>. Thermochemical conversion also includes pyrolysis, hydrolysis, reforming and liquefaction as shown in Figure 1.3. Pyrolysis and liquefaction convert biomass directly at high temperature to bio-oils, gases, and char, while steam reforming of bio-oil after fast pyrolysis requires noble metals as the catalyst (Mohanty et al., 2015). Typically, about 60 – 70 % of the weight of biomass is converted to bio-oil, while 13 - 15 % are from biochar and 13 – 25 % are from syngas.

Another alternative of renewable H<sub>2</sub> production is the biological conversion which requires less energy than the thermochemical conversion methods mentioned earlier. The biologically generated H<sub>2</sub>, or more commonly known as biohydrogen is of great interest due to its high energy content and sustainability. Biohydrogen can be biologically produced via a wide range of processes, such as direct biophotolysis, indirect biophotolysis, photo-fermentations and dark-fermentation. Direct

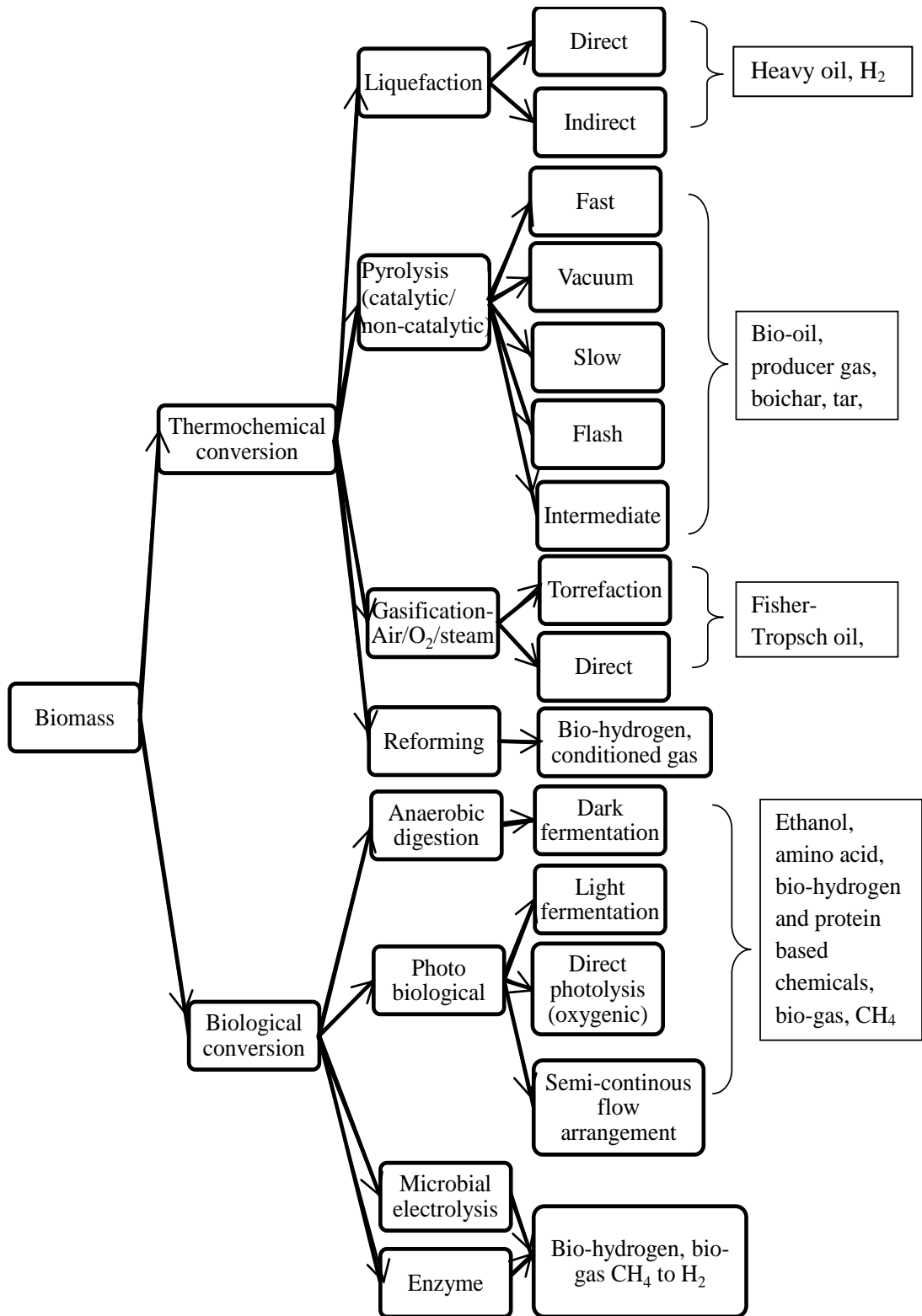
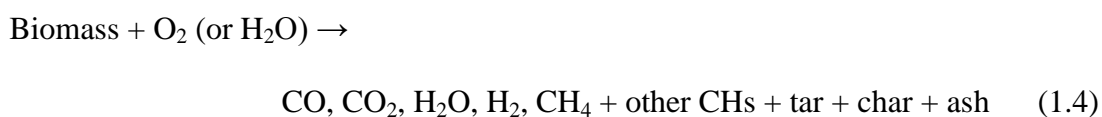


**Figure 1.3:** Different conversion routes of biomass into H<sub>2</sub> (Mohanty et al., 2015).

biophotolysis involves the photosynthetic reaction to convert solar energy into chemical energy using microalgae. The biophotolysis of water also can be indirectly achieved in serial reactions using cyanobacteria. H<sub>2</sub> production from microalgae is attractive since it produce H<sub>2</sub> from easily available water without the accumulation of CO<sub>2</sub> and more than 80 % of the theoretical solar energy conversion efficiency can be achieved. However, the H<sub>2</sub> production rate by cyanobacteria is few times higher than the H<sub>2</sub> production rate of green microalgae (Azwar et al., 2014). Equation for gasification of biomass is generally followed the reaction below (Balat et al., 2010);



In photo fermentation, the photosynthetic bacteria such as Purple Non-Sulfur bacteria can produce H<sub>2</sub> from organic acids and alcohol under sunlight. Without sunlight, dark fermentation usually employs anaerobic bacterial as well as some microalgae to produce more fermentation products besides H<sub>2</sub>, including CH<sub>4</sub>, CO<sub>2</sub>, CO and hydrogen sulphide (H<sub>2</sub>S) from carbohydrates. Since a great amount of acetic acid and/or butyric acids is also produced in dark fermentation, the acid can be further used as the supply for a photo fermentative process in the integrated system (Gandía et al., 2013).

Taking the H<sub>2</sub> production cost of SMR as the basis (\$2.08/kg), biomass pyrolysis and gasification appear to be viable since they only cost about \$ 1.50 - 2.20 to produce 1 kg of H<sub>2</sub>. Biological processes such as biophotolysis offers lower capital cost than SMR besides a reasonable production cost near to \$2/kg. H<sub>2</sub> production through biomass conversion is considered a carbon-neutral option although carbon



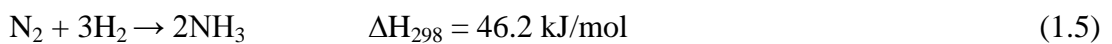
exists in the process (Bartels, 2008). This is because CO<sub>2</sub> is used in the growth of H<sub>2</sub> feedstocks such as plants and microorganisms. According to the finding of United Nations Environment Programme (Chandak, 2010), 140 billion metric tons of biomass is generated every year from agriculture and it is equivalent to approximately 50 billion tons of oil. Hence, H<sub>2</sub> production using bioresources is expected to grow dramatically in the near future. Table 1.1 shows the typical composition of gases from various processes.

**Table 1.1:** Typical composition of gases from various processes (Liew et al., 2013).

| Process              | Composition vol%, dry basis |                 |                |                 |      |       |
|----------------------|-----------------------------|-----------------|----------------|-----------------|------|-------|
|                      | H <sub>2</sub>              | CO <sub>2</sub> | N <sub>2</sub> | CH <sub>4</sub> | CO   | Other |
| SMR                  | 75.7                        | 8.1             | 0.2            | 0.5             | 15.5 | 0.0   |
| WGS                  | 31.7                        | 3.4             | 13.1           | 12.2            | 30.0 | 9.6   |
| Coal Gasification    | 29.4                        | 10.0            | 0.6            | 0.0             | 59.4 | 0.6   |
| Partial Oxidation    | 46.0                        | 4.3             | 1.4            | 0.3             | 47.0 | 1.0   |
| Biomass Gasification | 18.6                        | 15.7            | 56.0           | 0.6             | 8.7  | 0.4   |
| Biomass fermentation | 4.4                         | 16.5            | 56.8           | 4.2             | 14.7 | 3.4   |

## 1.2 Hydrogen Separation

Currently, a large number of H<sub>2</sub> production sites are designed for ammonia and methanol plants which require Nitrogen (N<sub>2</sub>): H<sub>2</sub> ratio of 3 : 1 and H<sub>2</sub> : CO ratio of 2 : 1, respectively. The ammonia synthesis reaction shown in equation (1.5) (Bartels, 2008).



It is customary to convert almost all CO to H<sub>2</sub> using WGS followed by CO<sub>2</sub> scrubbing and methanation for ammonia production, while CO<sub>2</sub> removal is not required for syngas utilization. However, the utilization of H<sub>2</sub> as the energy carrier in fuel cells for transportation and power generation requires H<sub>2</sub> with high purity. In addition, more alternatives for H<sub>2</sub> production using bioresources at low yield and rate have been developed in the recent years. H<sub>2</sub> separation and purification becomes an important topic.

Pressure swing adsorption (PSA) is the most common method used in H<sub>2</sub> separation. PSA is conducted using at least two adsorbent beds. One of the bed captures the impurities (CO, CO<sub>2</sub>, CH<sub>4</sub>, and water (H<sub>2</sub>O)) in the syngas stream or the product gas of WGS at high pressure (10 - 40 bar), while another bed releases the impurities at low pressure. In most of the applications, multiple beds are simultaneously utilized so that a continuous stream of H<sub>2</sub> with purity up to 99.9 % may be produced. The modern PSA units usually utilize 3 to 4 types of adsorbents to remove various kinds of impurities, namely silica gel or alumina for water separation, activated carbon for CO<sub>2</sub> capture as well as 5A zeolite for CH<sub>4</sub>, CO and N<sub>2</sub> removal (Ritter and Ebner, 2007). Nowadays, PSA with 12 adsorbent columns is commonly found and PSA with up to 16 columns for H<sub>2</sub> recovery close to 90 % has been patented (Grande, 2012). Over 500 PSA plants including the world's largest PSA unit have been designed and supplied by Linde, ranging from small plant sizes of a few hundred Nm<sup>3</sup>/h to a large scale plants of over 400 000 Nm<sup>3</sup>/h feed gas flow (PSA, 2016). Temperature swing adsorption (TSA) is different from PSA in term of desorption only, but it is not widely used because of the relatively long time for heating and cooling of sorbents. Electrical swing adsorption has been proposed as

well, but it is currently at the development stage. Cryogenic separation processes purify H<sub>2</sub> at extremely low temperatures when the production of moderately pure H<sub>2</sub> and highly pure CO from syngas are required. These processes use the difference of boiling temperatures among the feed components to achieve separation. H<sub>2</sub> has a higher relative volatility compared to other hydrocarbons, so a high H<sub>2</sub> recovery at moderate H<sub>2</sub> purities (95 % or less) can be achieved using a cryogenic system. Cryogenic separation processes are also applied to recover H<sub>2</sub> from other gas stream containing C<sub>2+</sub> liquid products (Ritter and Ebner, 2007). However, cryogenic distillation is quite expensive.

On the other hand, membrane processes such as Polysep membrane systems and PRISM membrane systems have been developed by UOP and Monsanto, respectively. These membrane systems are now sold by Air Products and Chemicals Inc. to recover H<sub>2</sub> from various refineries, petrochemical and chemical plants. Polymeric membranes, most likely polysulfone (PSf) in different shapes are utilized in both membrane separation systems. The spiral wound membranes are used in Polysep while the hollow fibers are used in PRISM. These membrane systems are able to achieve H<sub>2</sub> purity in the range of 70 to 99 vol.% with a H<sub>2</sub> recovery ranging from 70 to 95 % (Ritter et al., 2007). The H<sub>2</sub> permeates through the polymeric membranes via solution-diffusion and the preferential permeation of H<sub>2</sub> is achieved using the diffusivity selective membranes. This is because the kinetic diameter of H<sub>2</sub> (2.89 Å) is smaller than the kinetic diameter of other gases such as CO<sub>2</sub> (3.30 Å) (Li et al., 2015). An upper bound limit for the separation performance of polymeric membranes in H<sub>2</sub> purification can be predicted by Robenson. (2008) as shown in Figure 1.4. This upper bound shows the trade-off between permeability and

selectivity. This upper bound also represents the biggest challenge in gas separation using polymeric membranes (Ahmad and Hägg, 2013).

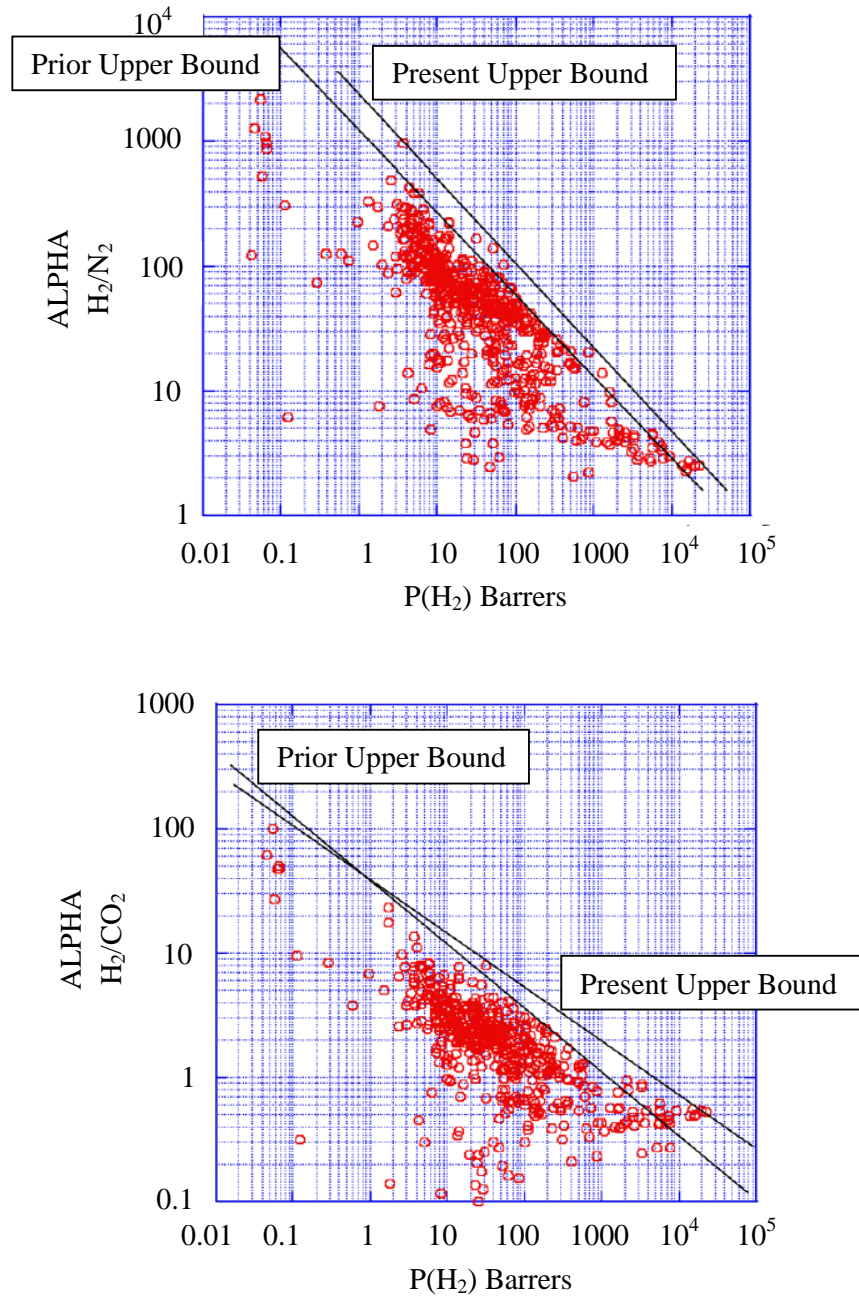


**Figure 1.4:** Upper bound correlation for  $H_2/N_2$  and separation  $H_2/CO_2$  (Robeson, 2008).

Table 1.2 below summarizes the performance comparison of H<sub>2</sub> separation by different separation process.

**Table 1.2:** The performance comparison of H<sub>2</sub> separation by different separation processes (Market, 2013).

| <b>Features</b>                 | <b>PSA</b>     | <b>Cryogenics</b>                          | <b>Membranes</b> |
|---------------------------------|----------------|--|------------------|
| H <sub>2</sub> purity           | 99.9 % +       | 90.0 – 96.0 %                              | 90.0 - 98.0 %    |
| H <sub>2</sub> recovery         | 75 – 92 %      | 90 – 98 %                                  | 85 – 95 %        |
| Feed pressure                   | 10 – 40 bar    | >5 - 75 bar                                | 20 – 160 bar     |
| Feed H <sub>2</sub> content     | >40 %          | >10 %                                      | > 25 – 50 %      |
| H <sub>2</sub> product pressure | Feed pressure  | Feed / low pressure                        | <<Feed pressure  |
| H <sub>2</sub> capacity         | 1 – 200 MMscfd | 5 – 60 MMscfd                              | < 50 MMscfd      |
| Pretreatment requirements       | None           | CO <sub>2</sub> , H <sub>2</sub> O removal | Minimum          |
| Multiple products               | No             | Liquid HCs                                 | No               |

The selection of H<sub>2</sub> separation techniques depends on several factors when they are integrated into the existing process such as SMR and coal gasification. The major factors are the process conditions (temperature and pressure), the product purity and recovery as well as the flexibility and efficiency of separation technique. However, biohydrogen requires the different selection criteria of H<sub>2</sub> separation techniques from SMR and gasification. This is because most of the biological production routes of H<sub>2</sub> involve the low temperature and pressure at a wide range of production scale. Among the separation techniques, membrane separation appears to be attractive especially when the options of H<sub>2</sub> production using bioresources have grown over the years. Membrane separation offers: (1) high energy efficiency, (2)

cost effectiveness per foot print, (3) simplicity in operation, and (4) environmentally friendly (Shao et al., 2009). More importantly, a wide spectrum of membrane material is available to fit different gas composition at varied temperature and pressure.

Besides polymeric membranes, palladium (Pd) based membranes are attractive alternatives to PSA and cryogenic separation. Pd based membrane was first commercialized by Johnson Matthey in 1964 to purify a H<sub>2</sub> rich-stream (Falco et al., 2011). A H<sub>2</sub> generator comprising of Pd membrane reactor fed with a methanol/water mixture was also developed by Johnson Matthey. However, Johnson Matthey which makes many gas purification products suited to light-emitting diode (LED) and compound semiconductor manufacturing exited the gas purification market. Johnson Matthey closed down the facility in West Chester, Pennsylvania in 2013 due to the slowdown in LED fabrication market (Johnson, 2013). Nevertheless, other companies continue to develop Pd based membranes for H<sub>2</sub> production and separation. For instance, Pall Corporation offers Pd-based membranes which are developed under the collaboration with Colorado School of Mines (Membrane, no date). Green Hydrotec has commercialized H<sub>2</sub> generator equipped with catalytic heater and Pd membrane tube in reformer (Hydrotec, 2010), while Fraunhofer IST is working with Plansee SE and Linde to develop Pd membranes on porous metal support (IST, 2012). The thickness of Pd membranes on support is typically in the order of 50 - 100 μm. The H<sub>2</sub> flux through Pd membranes is inversely proportional to the membrane thickness. Hence, the reduction of membrane thickness is important. The permeation of H<sub>2</sub> via Pd membrane involves the reversible adsorption of H<sub>2</sub> molecules at the Pd surface, followed by the rapid dissociation and diffusion of H<sup>+</sup>

ions into the metal lattice (Lewis, 1967). The permeated  $H^+$  ions recombine and desorbed from the Pd membrane. The Pd membranes work in a temperature range of 300 - 600 °C and they achieve a very high selectivity (>1000) and permeance compared to other types of membranes. Unfortunately, Pd is relatively expensive and Pd alloy membranes have been further developed (Al-Mufachi et al., 2015).

The  $H_2$  separation using membranes should not further increase the cost of  $H_2$  production and hinders the development of  $H_2$  economy.  $H_2$  separation using a membrane system with a cost less than \$1080/m<sup>2</sup> is the target of US Department of Energy (DOE) (Phair and Badwal, 2006). Besides economic consideration, the membrane should be selected based on the properties of product gas such as composition, pressure and temperature. The selectivity and the gas permeance of a membrane are the basic properties evaluated during the selection. The membrane separation system is more efficient by incorporating the membrane with higher selectivity, so that a lower driving force (pressure ratio) is required and a cheaper operating cost is accomplished. A smaller membrane area is needed when a membrane with higher permeance is selected, leading to a reduced capital cost. Without the satisfactory selectivity and permeance, the permeate gas needs to be recompressed and recycled back to the membrane separation system designed with multiple stages. The recycle cascades require additional compressor and it is highly energy demanding. Therefore, it may overturn the economic advantages of membrane-based separations compared to PSA or cryogenic distillation. With the satisfactory selectivity and permeance,  $H_2$  separation membranes showed great potential to reduce separation cost by over 30 % compared to PSA (Gupta, 2008).

### 1.3 Problem Statement

Asian countries produce almost 85 % biomass waste in the world and the waste mainly located in Malaysia and Indonesia (Pudukudy et al., 2014). Hence, H<sub>2</sub> production from the biomass waste is expected to grow in this region. Gasification (Samiran et al., 2016) and fermentation (Ahmad et al., 2016) are the most extensively studied methods for H<sub>2</sub> production from oil palm waste and palm oil mill effluent, respectively. Currently, no membrane meets all the criteria required in the purification of H<sub>2</sub> produced from biomass. Pd membranes can be easily integrated into the gasification plant because Pd membranes can separate H<sub>2</sub> from CO<sub>2</sub> within the high temperature range of 300 - 600 °C (Al-Mufachi et al., 2015). H<sub>2</sub>-embrittlement cracking only occurs when Pd membranes are used in H<sub>2</sub> separation below 300 °C and 20 bar (Falco et al., 2011). However, Pd membranes are not the perfect solution due to the high cost of Pd and alloys. Polymeric membrane can be used to purify the biohydrogen at low temperature and pressure, but most of the polymeric membranes including PSf membrane cannot surpass the Robeson upper bound limit for H<sub>2</sub> separation from N<sub>2</sub> or CO<sub>2</sub>.

In recent years, mixed matrix membranes (MMMs) have been extensively studied and developed (Li et al., 2015). MMMs comprise of dispersed particles and the continuous polymer matrix to surpass the Robeson upper bound limit. The solution-diffusion limitation of the polymeric membranes could be easily overcome by incorporating various types of zeolites, silica, carbon molecular sieves, carbon nanotubes, and metal organic frameworks (Li et al., 2015). Pd nanoparticles are proposed to be incorporated into PSf membrane in this work in order to develop MMMs that separate H<sub>2</sub> satisfactorily and economically. However, the use of Pd



nanoparticles to engineer MMMs for gas separation has not been reported to the best knowledge. The Pd nanoparticles have been incorporated into polymeric matrix as catalyst (Emin et al., 2014, Gu et al., 2015). In addition, they have been used in H<sub>2</sub> sensing (Wadell et al., 2014) and supported on porous absorbent for H<sub>2</sub> storage (Konda and Chen, 2016). In the development of the H<sub>2</sub> selective MMMs, Pd nanoparticles appear to be a promising choice since they have high affinity for H<sub>2</sub> sorption. Pd nanoparticles are able to absorb large volumetric quantities of H<sub>2</sub> at room temperature and atmospheric temperature by forming palladium hydride (PdH<sub>x</sub>) (Konda and Chen, 2016).

The improvement on the separation performance of MMMs not only depends on the selection of inorganic particle, but also relies on the loading of inorganic particle. Particle agglomeration can cause the adverse effects on membrane separation performance. Membrane separation is also affected by the nature and degree of interfacial adhesion between the polymer and particles. Unlike other inorganic filler, Pd nanoparticles can be kinetically stabilized using electrostatic and/or steric forces of a stabilizer without affecting the functionality and surface area of Pd nanoparticles. More importantly, the stabilizers such as polyvinylpyrrolidone (PVP) or polyethylene glycol (PEG) can introduce microvoids between polymeric matrix and Pd fillers to avoid pore blockage or diffusion hindrance. These stabilizers are common additive in gas separation membranes as well (Loloei et al., 2015, Aroon et al., 2010). Thus, it is proposed to utilize the Pd nanoparticles in appropriate stabilizers to attain the desired nanoparticles size and prevent from aggregating and allow one to isolate the nanoparticles.

For high temperature separation, glassy membranes including PSf membrane age faster at higher temperature and experience permeability loss (Huang and Paul, 2005). The thinner membranes tend to age faster than the thick membranes. Hence, the application of glassy membranes such as PSf membrane is limited by the high temperature of H<sub>2</sub> rich gas produced from biomass gasification. The investigation of temperature effects on Pd nanoparticles dispersed in polymer matrix is also limited by these reasons. Polybenzimidazole (PBI) with a very high melting point should be selected to engineer MMMs for the separation of H<sub>2</sub> from hot gas. Although conventional PBI showed high selectivity, its closed and packed structure is the major constrain for the gas permeation. Hence, it is also interesting to study the effects of different stabilizers of Pd nanoparticles such as PEG and PVP which work as the membrane additives on PBI membranes (Loloei et al., 2015). The incorporation of Pd nanoparticles into PBI thin film allows further investigation of the temperatures effects on the functionality of Pd nanoparticles dispersed in polymer matrix. The application of Pd in H<sub>2</sub> storage and separation are affected by temperature as reported by many works (Sheng et al., 2014, Falco et al., 2011), but the effects of temperature on MMMs incorporated with Pd nanoparticles in H<sub>2</sub> separation remain unknown.

#### **1.4 Objectives**

The present research has the following objectives:

1. To synthesize and characterize PSf and PBI membrane incorporated with Pd nanoparticles.
2. To study the effects of Pd nanoparticles, stabilizer and temperature on the H<sub>2</sub> separation performance of PSf and PBI MMMs.

3. To perform a feasibility study using mathematical model in H<sub>2</sub> purification for biohydrogen system using Polymath software.

### **1.5 Scope of Study**

This study basically focuses on the development of MMMs incorporated with Pd nanoparticles for H<sub>2</sub> separation. The Pd nanoparticles were synthesized using the inversed microemulsion. There were two stabilizers used in this study, namely PEG and PVP. These polymers were chosen by considering the stability of Pd colloid precursor, the solvent and the ability of the polymer to stabilize the reduced Pd nanoparticles. The synthesized Pd nanoparticles were characterized using Transmission Electron Micrographs (TEM), X-ray Diffraction (XRD) and Temperature Programmed Reduction (TPR) before being blended into PSf polymer matrix. The MMMs incorporated with Pd nanoparticles were synthesized using the common method, phase inversion. The Pd nanoparticles were blended into the polymer solution prior to casting and phase inversion.

The common H<sub>2</sub> separation membrane material, PSf has been chosen as the first polymer matrix to develop the MMMs. The Pd nanoparticles synthesized using PEG and PVP as the stabilizer were separately incorporated into the PSf matrix to form two types of PSf(Pd) MMMs. Besides the effects of stabilizer, the effects of Pd nanoparticles loading on membrane properties were studied using TPR, XRD, Fourier Transform Infrared (FTIR) Spectroscopy, Scanning Electron Microscope (SEM) and Energy Dispersive X-ray (EDX). The control membrane, the neat PSf membrane was also synthesized and characterized to compare the effects of stabilizers and Pd loading on PSf MMMs. PSf(Pd/PEG) and PSf(Pd/PVP) MMMs

were further tested for gas separation to study the compatibility of PSf polymer, PEG or PVP stabilizer and Pd nanoparticles. In addition, the separation test was used to determine the appropriate loading of Pd nanoparticles in PSf. The separation of H<sub>2</sub> from N<sub>2</sub> and CO<sub>2</sub> gases using MMMs membrane were the second focus in this study.

In order to improve the separation performance of MMMs and their stability at the high temperature (100 - 150 °C), PBI has been chosen as the second polymer. Similar to the PSf MMMs, the Pd nanoparticles synthesized using stabilizer such as PEG and PVP was incorporated in the PBI matrix to form PBI MMMs. The compatibility between PBI matrix, PEG or PVP stabilizer and Pd nanoparticles were studied. Besides the effects of stabilizer, the effects of Pd loading on the membrane morphology and separation performance were investigated. The effects of temperature on H<sub>2</sub> separation performance of a selected PBI(Pd) MMMs were also considered. All the fabricated PBI(Pd) MMMs were characterized via XRD, SEM, FTIR, EDX and TPR. The chosen PBI MMMs (selected based on their separation performance) were further tested at high operating temperature (200 - 300 °C) to study the effects of temperature.

In addition, the feasibility of PBI(Pd) MMMs in the purification of H<sub>2</sub> produced from fermentation and biomass gasification were mathematically evaluated. The membrane feasibility was measured in terms of membrane area, product purity and gas recovery.

## 1.6 Organization of the Thesis

This thesis comprises of five chapters as listed in the table of content. It provides all the details and findings of this research. Each chapter contains the important knowledge and information as listed below.

Chapter one (Introduction) presents the overview of H<sub>2</sub> demand in various applications and their production using different routes as well as resources. The comparison between the conventional separation methods and the advantages using membrane separation has been highlighted. Besides the polymeric membranes, the general overview on Pd membranes and their application in H<sub>2</sub> separation have been briefly described to give a fundamental view. Next, the problem statements of the study are also being discussed. Then, the research objectives are listed and the scopes of study are thoroughly explained. Lastly, the organization of the thesis is specified in the last section of this chapter.

Chapter two (Literature Review) is devoted to an extensive literature review from previous to recent studies. The first part of the literature focuses H<sub>2</sub> selective membrane. Subsections of this part explain the general overview on PSf and PBI as membrane material including its characteristic and their separation performance. Next, the overview on inorganic membrane based on dense metallic and microporous membrane has also been explained. The review is focused further on the MMMs for H<sub>2</sub> separation, which involve the incorporation of different type of filler. A review study was done on the effect of stabilizer, filler loading and high operating temperature on MMMs performance. In the next section, the application of membrane in biohydrogen system has been discussed. The last segment gives

attention on Pd nanoparticles which involves the discussion on their uses and synthesis method.

Chapter three (Research Methodology) presents the detail of materials and chemicals used through this research study. This is followed by the detailed experimental procedures, which include the synthesis of Pd nanoparticles, the fabrication of PSf and PBI MMMs, characterization method and gas performance analysis. Details on the experimental set up are also elaborated in this chapter. In the last section, the mathematical model and membrane process simulation are listed.

Chapter four (Result and Discussion) is the core of this thesis, which address the three objectives as listed in Chapter 1. The research findings and results are presented and extensively discussed. The first section, presented the preparation and characterization of PSf MMMs incorporated with Pd nanoparticles by using PEG and PVP as stabilizer. The second section investigated the effect of stabilizer and Pd nanoparticles on the performance of PSf MMMs in H<sub>2</sub> separation. The third section presented the preparation and characterization of PBI MMM with Pd stabilized by PEG and PVP. The last section discussed the effects of Pd, stabilizer and temperature on the H<sub>2</sub> separation performance of PBI MMMs. Besides, a feasibility study on H<sub>2</sub> purification that been conducted based on fermentation and gasification system also has been studied in this section.

Chapter five (Conclusions and Recommendation) concludes all the major findings obtained in the result and discussions in this present study. At the end of the

thesis, suggestion, recommendation that describe future improvements on present study are presented.